ACADEMIC PRESS

Available online at www.sciencedirect.com

SCIENCE DIRECT®

Journal of Computational Physics 187 (2003) 47–67

JOURNAL OF COMPUTATIONAL PHYSICS

www.elsevier.com/locate/jcp

Multi-scale finite-volume method for elliptic problems in subsurface flow simulation

P. Jenny, S.H. Lee *, H.A. Tchelepi

ChevronTexaco Exploration and Production Technology Company, 6001 Bollinger Canyon Road, San Ramon, CA 94583-0932, USA

Received 2 January 2002; received in revised form 5 November 2002; accepted 10 January 2003

Abstract

In this paper we present a multi-scale finite-volume (MSFV) method to solve elliptic problems with many spatial scales arising from flow in porous media. The method efficiently captures the effects of small scales on a coarse grid, is conservative, and treats tensor permeabilities correctly. The underlying idea is to construct transmissibilities that capture the local properties of the differential operator. This leads to a multi-point discretization scheme for the finite-volume solution algorithm. Transmissibilities for the MSFV have to be constructed only once as a preprocessing step and can be computed locally. Therefore this step is perfectly suited for massively parallel computers. Furthermore, a conservative fine-scale velocity field can be constructed from the coarse-scale pressure solution. Two sets of locally computed basis functions are employed. The first set of basis functions captures the small-scale heterogeneity of the underlying permeability field, and it is computed in order to construct the effective coarse-scale transmissibilities. A second set of basis functions is required to construct a conservative fine-scale velocity field. The accuracy and efficiency of our method is demonstrated by various numerical experiments.

Keywords: Subsurface flow; Multi-scale physics; Upscaling; Finite-volume

1. Introduction

The level of detail in reservoir description exceeds the computational capability of existing reservoir simulation. This resolution gap is usually tackled by upscaling the fine-scale description to sizes that can be treated by a full-featured simulator. In upscaling, the original model is coarsened using a computationally inexpensive process. In flow-based methods [5], the process is based on single-phase flow. The simulation study is then performed using the coarsened model. These upscaling methods have proved quite successful. However, it is not possible to have a priori estimates of the errors that are present when complex flow processes are investigated using coarse models constructed via simplified settings.

* Corresponding author. Tel.: 1-925-842-6392; fax: +1-925-842-6283.
E-mail addresses: pjnn@chevrontexaco.com (P. Jenny), seon@chevrontexaco.com (S.H. Lee), htch@chevrontexaco.com (H.A. Tchelepi).

0021-9991/03/$ - see front matter
doi:10.1016/S0021-9991(03)00075-5

Various fundamentally different multi-scale approaches for flow in porous media have been proposed to accommodate the fine-scale description directly. As opposed to upscaling, the multi-scale approach targets the full problem with the original resolution. The methodology is based on resolving the length and time-scales of interest by maximizing local operations. Arbogast [1] and Arbogast and Bryant [2] presented a mixed finite-element method, where the fine-scale effects are localized by a boundary condition assumption at the coarse element boundaries. Then the small-scale influence is coupled with the coarse-scale effects by numerical Greens functions. Hou and Wu [8] employed the finite-element approach and constructed specific basis functions which capture the small scales. Again, localization is achieved by boundary condition assumptions for the coarse elements. To reduce the effects of these boundary conditions an oversampling technique can be applied. Recently, Chen and Hou [4] applied these ideas in combination with a mixed finite-element approach. Another approach by Beckie et al. [3] is based on large eddy simulation (LES) techniques which are commonly used for turbulence modeling.

Here a new multi-scale finite-volume (MSFV) approach is proposed which employs ideas from the flux-continuous finite-difference (FCFD) scheme developed by Lee et al. [10] for 2D, Lee et al. [11] for 3D, and later implemented in a multi-block simulator by Jenny et al. [9]. We also follow some principal ideas presented by Hou and Wu [8] and Efendiev et al. [6]. Advantages of our method are that it fits nicely into a finite-volume framework, allows for computing effective coarse-scale transmissibilities, treats tensor permeabilities properly, and is conservative at the coarse and fine scales. We will show that the method is computationally efficient and well suited for massively parallel computation. We also discuss how it can be applied to 3D unstructured grids and extended to multi-phase flow.

In Section 2 the flow problem is briefly introduced and in Section 3 the multi-scale finite-volume method is explained. Implementation and efficiency of the method are discussed in Sections 4 and 5, and numerical results are presented in Section 6. Finally, application to unstructured grids and multi-phase flow are discussed in Section 7. Summary and conclusions are given in Section 8.

2. Flow problem

We study the following elliptic problem:

$$\nabla \cdot (\lambda \cdot \nabla p) = f \quad \text{on } \Omega, \tag{1}$$

where p is the pressure and λ is the mobility (permeability, $\mathbf{K}$, divided by the fluid viscosity, μ). The source term f represents wells and in the compressible case time derivatives. The permeability heterogeneity is a dominant factor in dictating the flow behavior in natural porous formations. The heterogeneity of $\mathbf{K}$ is usually represented as a complex multi-scale function of space. Moreover, $\mathbf{K}$ tends to be a highly discontinuous full tensor. Resolving the spatial correlation structures and capturing the variability of permeability requires highly detailed description. The velocity $\mathbf{u}$ is related to the pressure field through Darcy's law,

$$\mathbf{u} = -\lambda \cdot \nabla p. \tag{2}$$

On the boundary $\partial\Omega$ the flux $q = \mathbf{u} \cdot v$ is specified, where v is the boundary unit normal vector pointing outward. Eqs. (1) and (2) describe incompressible flow in porous media. These equations apply for both single and multi-phase flows when appropriate interpretations of the mobility coefficient λ and velocity are made. This elliptic problem is a simple, yet representative, description of the type of systems that must be handled efficiently by a subsurface flow simulator. Moreover, the ability to handle this limiting case of incompressible flow ensures that compressible systems can be treated consistently.

3. Multi-scale finite-volume (MSFV) method

We derive a multi-scale approach which results in effective transmissibilities for the coarse-scale problem. Once the transmissibilities are constructed, the method, which employs ideas from the flux-continuous finite-difference (FCFD) scheme developed by Lee et al. [11], does not differ from a finite-volume scheme using multi-point stencils for flux discretization. The approach is conservative and treats tensor permeabilities correctly. It can be easily applied by existing finite-volume codes, and once the transmissibilities are computed, it is computationally very efficient. In computing the effective transmissibilities, we employ similar closure assumptions as in the multi-scale finite-element method of Hou and Wu [8]. It is a crucial property of our multi-scale method that two sets of basis functions are employed. The first set has to be computed in order to construct transmissibilities. A second set of locally computed basis functions allows reconstruction of the fine-scale velocity field from the coarse solution. It is important that we design these basis functions such that the reconstructed fine-scale solution is fully consistent with the transmissibilities, and that it satisfies the proper mass balance on the small scale.

3.1. Finite-volume method

Here, we briefly explain the cell-centered finite-volume method. To solve problem (1) we partition Ω into smaller volumes $\{\bar{\Omega}_i\}$. A finite-volume solution then satisfies

$$\int_{\bar{\Omega}_i} \nabla \cdot \mathbf{u}\,\mathrm{d}\Omega = \int_{\partial\bar{\Omega}_i} \mathbf{u} \cdot \bar{\nu}\,\mathrm{d}\Gamma = -\int_{\bar{\Omega}_i} f\,\mathrm{d}\Omega, \tag{3}$$

for each volume $\bar{\Omega}_i$, where $\bar{\nu}$ is the unit normal vector of the volume interface $\partial\bar{\Omega}_i$ pointing outward. The challenge is to find a good approximation for $\mathbf{u} \cdot \bar{\nu}$ at $\partial\bar{\Omega}_i$. In general the flux is expressed as

$$\mathbf{u} \cdot \bar{\nu} = \sum_{k=1}^{n} T^k \bar{p}^k. \tag{4}$$

Eq. (4) is a linear combination of the pressure values, $\bar{p}$, in the volumes of the domain. The total number of volumes is n and T^k denotes transmissibility. By definition, the fluxes (4) are continuous across the interfaces and as a result the finite-volume method is conservative.

3.2. Construction of the effective transmissibilities

The MSFV method results in multi-point stencils for the coarse-scale fluxes. For the following description, we use the orthogonal 2D grid shown in Fig. 1 and assume that there exists an underlying fine grid containing the fine-scale permeability information. To compute the transmissibilities a dual grid is

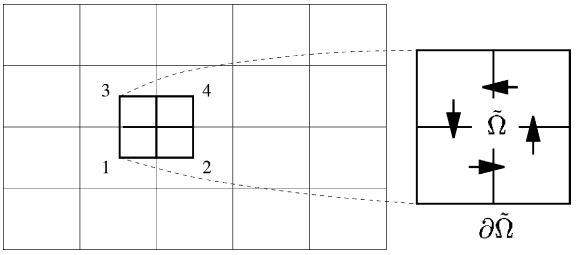

Fig. 1. Coarse 2D grid with dual volume $\tilde{\Omega}$.

used, which is analogous to our previous FCFD method [10,11]. A control volume of the dual grid, $\tilde{\Omega}$, is constructed by connecting the volume mid-points of four adjacent grid-blocks. To relate the fluxes across the volume interface segments which lie inside $\tilde{\Omega}$ to the finite-volume pressures $\bar{p}^k$ $(k = 1,4)$ in the four adjacent volumes, we define the local problem

$$\nabla \cdot (\lambda \cdot \nabla p) = 0 \quad \text{on } \tilde{\Omega}. \tag{5}$$

For an elliptic problem, Dirichlet or Neumann boundary conditions are to be specified on $\partial\tilde{\Omega}$. Ideally, the imposed boundary conditions should approximate the true flow conditions experienced by the sub-domain in the full system. Obviously, these boundary conditions can be time- and flow-dependent. Since the sub-domain is embedded in the whole system, Wallstrom et al. [12] found that a constant pressure condition at the sub-domain boundary tends to overestimate flow contributions from high permeability areas. If the correlation length of permeability is not much larger than the grid size, the flow contribution from high permeability is not proportional to the nominal permeability ratio. The transmissibility between two grids is a harmonic mean that is closer to the lower permeability. As a result, uniform flux conditions along the boundary often yield much better numerical results for a sub-domain problem than linear or constant pressure conditions. Hou and Wu [8] also proposed solving a reduced problem

$$\frac{\partial}{\partial x_t}\left(\lambda_{ij}\frac{\partial p}{\partial x_j}\right)_t = 0, \tag{6}$$

to specify the boundary conditions for the local problem. The subscript t denotes the component parallel to the boundary of the dual control volume $\tilde{\Omega}$ (for Eq. (6) and the following part of this paper we use the Einstein summation convention). The elliptic problem on $\tilde{\Omega}$ with boundary conditions (6) on $\partial\tilde{\Omega}$ can be solved by any appropriate numerical method. In order to obtain a solution that depends linearly on the pressures $\bar{p}^k$ $(k = 1,4)$, we solve four elliptic problems, one for each cell-center pressure. For instance, to get the solution for pressure $\bar{p}^1$ we set $\bar{p}^k = \delta_{1k}$. The four solutions are our dual basis functions $\tilde{\Phi}^k$ $(k = 1,4)$ in $\tilde{\Omega}$, and the solution of the local elliptic problem in $\tilde{\Omega}$ is the linear combination

$$p = \sum_{k=1}^{4} \bar{p}^k \tilde{\Phi}^k. \tag{7}$$

Accordingly, the flux q across the volume interfaces can be written as a linear combination

$$q = \sum_{k=1}^{4} \bar{p}^k q^k, \tag{8}$$

where q^k $(k = 1,4)$ are the flux contributions from the corresponding dual basis functions. Given all $\tilde{\Phi}^k$ $(k = 1,4)$ from all $\tilde{\Omega}$. We compute the effective transmissibilities, which can be used for finite-volume simulations, by assembling the integral flux contributions across the volume interfaces.

Note that the domain $\tilde{\Omega}$ can have any fine-scale distribution of λ. Of course the boundary condition given by (6) is an approximation that decouples the local problems. The MSFV and global fine-scale solutions are identical, only if (6) happens to capture the exact fine-scale pressure solution. However, the numerical experiments clearly indicate that Eq. (6) is an excellent approximation of the boundary condition.

Although the MSFV approach is a finite-volume method, it strongly resembles the multi-scale finite-element method by Hou and Wu [8]. The construction of the dual basis functions is almost identical, though in the MSFV method they are represented on the dual grid. The main difference is that the MSFV method is a cell-centered finite-volume scheme and is conservative. On the other hand, the mass matrix in the multi-scale finite-element method is constructed based on the variational principle and does not ensure

local conservation. In the following section we will illustrate the importance of a fine-scale velocity field that is conservative.

3.3. Reconstruction of a conservative fine-scale velocity field

Fluxes across the coarse volume interfaces can be accurately computed by multi-scale transmissibilities. In some cases one is also interested in accurately representing the small-scale velocities (e.g., to predict the distribution of solute transported by the fluid). A straightforward way would be to use the dual basis functions of (7), but then the reconstructed fine-scale velocity field is in general discontinuous at the volume interfaces of the dual grid. Therefore, large errors can occur in the divergence field, and local mass balance is violated. Note that mass conservation is always satisfied for the coarse solution.

Here, we describe how to construct a second set of local basis functions that is fully consistent with the fluxes across the volume interfaces given by the dual basis functions. This second set of basis functions allows us to reconstruct a conservative fine-scale velocity field. Fig. 2 shows the coarse grid with nine adjacent volumes (denoted by the numbers 1–9) and the corresponding dual grid (four of the volumes of the dual grid are denoted by the letters A, B, C and D). Also shown is the underlying fine grid. To explain the reconstruction of the fine-scale velocity, we focus on the mass balance of volume 5. The coarse solution together with the dual basis functions provide us with the fine-scale fluxes q across the interface of volume 5. To obtain a proper representation of the fine-scale velocity field in coarse volume 5, we ensure that (i) the fine-scale fluxes across an interface of coarse volume 5 are matching, and (ii) the divergence of the fine-scale velocity field within the coarse volume satisfies

$$\nabla \cdot \mathbf{u} = \frac{\int_{\partial \bar{\Omega}_5} q \, \mathrm{d}\Gamma}{\int_{\bar{\Omega}_5} \mathrm{d}\Omega}, \tag{9}$$

where $\bar{\Omega}_5$ is the coarse volume. The fine-scale flux q across the boundary of volume 5 depends on the coarse pressure solutions in volumes 1–9. Therefore, the fine-scale velocity field within volume 5 can be expressed as a superposition of basis functions Φ^i $(i = 1, 9)$. With the help of Fig. 3, which depicts the needed dual volumes, we describe the construction of the fine-scale basis functions Φ^i. Each coarse volume pressure $\bar{p}^i$ $(i = 1, 9)$ contributes to the fine-scale flux q. For example, let the contribution of the pressure in volume 2

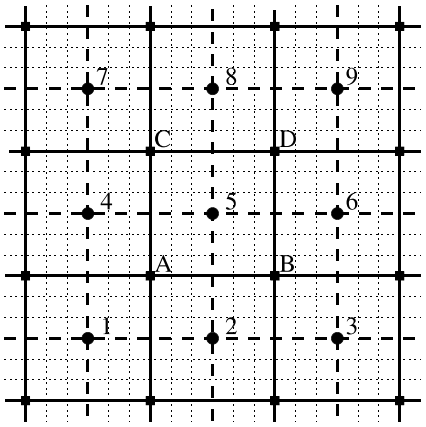

Fig. 2. Coarse grid with nine adjacent coarse volumes (bold solid lines) with the corresponding dual grid (bold dashed lines); also shown is the underlying fine grid (thin dotted lines).

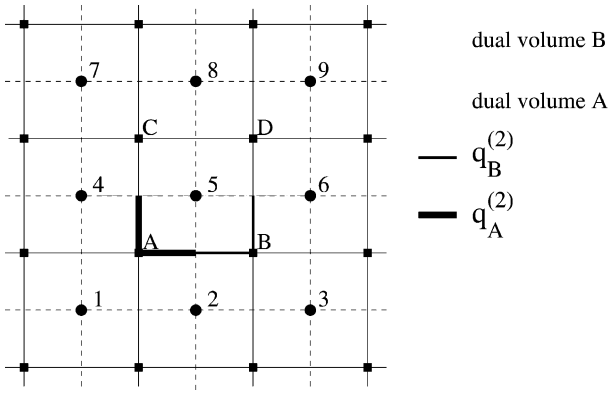

Fig. 3. Flux contributions $q_A^{(2)}$ and $q_B^{(2)}$ from the pressure in volume 2.

be $q^{(2)}$. Note that $q^{(2)}$ is composed of contributions $q_A^{(2)}$ and $q_B^{(2)}$ coming from the dual basis functions associated with node 2 of volume A and volume B, respectively. To compute the fine-scale basis function associated with the pressure in volume i we set $\bar{p}^j = \delta_{ij}$, and construct the pressure field given by

$$p = \sum_{k\in\{A,B,C,D\}} \sum_{j=1}^{9} \bar{p}^j \tilde{\Phi}_k^j. \tag{10}$$

From the pressure field we compute the fine-scale fluxes q. These fluxes provide the proper boundary condition for computing the fine-scale basis function Φ^i. To solve the elliptic problem

$$\nabla \cdot (\lambda \cdot \nabla p) = f' \quad \text{on } \bar{\Omega}_5, \tag{11}$$

with the boundary conditions described above, we first have to ensure solvability. This is achieved by setting

$$f' = \frac{\int_{\partial\bar{\Omega}_5} q \,\mathrm{d}\Gamma}{\int_{\bar{\Omega}_5} \mathrm{d}\Omega}, \tag{12}$$

which is an equally distributed source term within $\bar{\Omega}_5$. Finally, the solution of the elliptic problem, (11) and (12), is the fine-scale basis function for volume 5 associated with the pressure in volume i. The small-scale velocity field is extracted from the superposition

$$p = \sum_{j=1}^{9} \bar{p}^j \Phi_5^j. \tag{13}$$

It is important to note that for incompressible flow, this velocity field is divergence free everywhere. We just showed that computing the fine-scale basis functions requires solving nine small elliptic problems, which are of the same size as those for the transmissibility calculations. Note that this step is a preprocessing step and has to be done once only. Furthermore, the construction of the fine-scale basis functions is independent and therefore perfectly suited for parallel computation. The reconstruction of the fine-scale velocity field is a simple superposition and is performed only in regions of interest.

4. Implementation of the MSFV method

In this section we discuss the necessary steps and implications on the data structure when the MSFV method is implemented. The algorithm consists of six major parts:

1. Computation of transmissibilities for coarse-scale fluxes.
2. Construction of fine-scale basis functions Φ.
3. Computation of the coarse solution at the new time level.
4. Reconstruction of the fine-scale velocity field in regions of interest.
5. Solution of the transport equations.
6. Re-computation of transmissibilities (part 1) and fine-scale basis functions (part 2) in regions where the total mobility changed.

Parts 1–4 describe a two-scale approach. The methodology can be applied recursively with successive levels of coarsening. In cases of extremely fine resolution [7], this multi-level approach should yield scalable solutions. Parts 5 and 6 account for transport and mobility changes due to evolving phases (see Section 7.3) and are not discussed further in this paper.

Part 1 is a preprocessing step. The transmissibility calculations can be done in a stand alone module (T-module) and are well suited for parallel computation. The transmissibilities can be written to a file for use by any finite-volume simulator that can handle multi-point flux discretization. In order to follow the descriptions of Section 3.2 one has to do the following: The fine-scale grid with the permeability field and the coarse finite-volume grid have to be passed into the T-module, the dual control volumes have to be constructed (one for each node of the coarse grid), and for each dual control volume $\tilde{\Omega}$ the dual basis functions $\tilde{\Phi}$ have to be constructed by solving local elliptic problems within $\tilde{\Omega}$. Therefore the permeability field on the fine grid is used, and the boundary conditions (6) are applied. In cases where the fine and coarse grids are nonconforming (e.g., if unstructured grids are used), oversampling can be applied as discussed in Section 7.2. Finally, the integral fluxes across the single volume interfaces can be extracted from the dual basis functions $\tilde{\Phi}$ and by assembling them one obtains the MSFV-transmissibilities. Part 1 can be viewed as an upscaling procedure. That is, the constructed coarse solutions are designed to account, in some manner, for the fine-scale description of the permeability in the input model. Thus, part 1 is a separate preprocessing step to coarsen the original model to a size manageable by a conventional reservoir simulator.

Part 2, which can be isolated in a separate Φ-module, is only necessary if one is interested in reconstructing the fine-scale velocity field from the coarse solution. As described in Section 3.3, if the dual basis functions are used in reconstructing the fine-scale velocity field, large mass balance errors occur. Here we describe the steps necessary to compute the fine-scale basis functions Φ, which can be used to reconstruct a conservative fine-scale velocity field. The procedure, which follows the description of Section 3.3, has to be performed only once at the beginning of the simulation and is well suited for parallel computation. The fine-scale grid with its corresponding permeability field, the coarse finite-volume grid and the dual basis functions $\tilde{\Phi}$ are passed into the Φ-module. For each adjacent dual volume $\tilde{\Omega}$ of volume $\bar{\Omega}$, local elliptic problems have to be solved within $\bar{\Omega}$. The boundary conditions are obtained from the dual basis functions $\tilde{\Phi}$ as described in Section 3.3. Finally the result is a set of fine-scale basis functions Φ which must be stored. In many cases the fine-scale velocity field has to be reconstructed in certain regions only.

Part 3 can be performed by any multi-point stencil finite-volume code by using the MSFV-transmissibilities for the flux calculation. These coarse fluxes effectively capture the large-scale behavior of the solution without resolving the small scales.

Part 4 is straight forward. Reconstruction of the fine-scale velocity field in regions of interest is achieved by superposition of the fine-scale basis functions Φ as described in Section 3.3.

Of course, many variations of the MSFV method can be devised. It is important, however, that construction of the transmissibilities and fine-scale basis functions Φ can be done separate from the simulator. Next, we analyze the computational efficiency of the MSFV method.

5. Computational efficiency

In order to analyze the computational efficiency of the MSFV method we introduce the following definitions:

n_v	number of volumes of the fine grid
n_V	number of volumes of the coarse grid
n_N	number of nodes of the coarse grid
n_t	total number of time steps
a_N	average number of adjacent coarse volumes to a coarse node
a_V	average number of adjacent coarse volumes to a coarse volume
$t_l(n)$	CPU time to solve a linear system with n unknowns
t_m	CPU time for one multiplication

and assume that $t_l(n) = ct_m n^\alpha$, where c and α are constants. It is also assumed that β is the average fraction of the reservoir for which the fine-scale velocity has to be reconstructed each time step. We consider one phase flow only and therefore the computational cost of parts 5 and 6 in the previous section are not discussed. Next the required CPU times for the various parts of the algorithm are estimated.

For part 1, there are $n_N a_N$ problems with an average size of n_v/n_V to be solved. Therefore the estimated CPU time for the transmissibility calculations is

$$t_1 \approx n_N a_N c t_m \left(\frac{n_v}{n_V}\right)^\alpha, \tag{14}$$

which does not include oversampling. The work required to reassemble the fluxes to get the transmissibilities is assumed to be negligible. For part 2, $n_V(a_V + 1)$ problems with an average size of n_v/n_V must be solved. The estimated CPU time for the transmissibility calculations is

$$t_2 \approx n_V(a_V + 1) c t_m \left(\frac{n_v}{n_V}\right)^\alpha, \tag{15}$$

which ignores oversampling. Part 3 requires the solution of a coarse problem of size n_V. The estimated time is

$$t_3 \approx c t_m (n_V)^\alpha n_t. \tag{16}$$

In part 4, the fine-scale velocity field has to be reconstructed each time step for a fraction β of the whole reservoir. This is done by superposition and the required CPU time is

$$t_4 \approx t_m n_v (a_V + 1) n_t \beta. \tag{17}$$

Parts 1, 2 and 4 are well suited for parallel processing.

Example. Consider a structured $300 \times 300 \times 300$ fine grid. Let the coarse grid dimension be $30 \times 30 \times 30$. Then $n_v = 2.7 \times 10^7$, $n_V = 2.7 \times 10^4$, $n_N = 29,791$, $a_N = 8$ and $a_V = 26$. We take $c \approx 10$, $\alpha \approx 1.5$ and $\beta \approx 0.2$ and get

Table 1
Ratio of CPU times for the fine solution and the MS solution dependent on the number of time steps n_t

n_t	t_f/t_{ms}
1	5
10	46
100	432
1000	2828
10,000	6355

$$t_1 \approx 7.5 \times 10^{10} t_m,$$
$$t_2 \approx 2.3 \times 10^{11} t_m,$$
$$t_3 \approx 4.4 \times 10^{7} t_m n_t,$$
$$t_4 \approx 1.5 \times 10^{8} t_m n_t.$$

The estimated time to solve the fine problem is

$$t_f \approx 1.4 \times 10^{12} t_m n_t.$$

Table 1 shows the estimated speedup for different time-step numbers (without considering parallel computing). Of course this result depends strongly on the assumptions, especially about the value for α, but it is apparent that the MSFV method provides a very efficient way to obtain an accurate fine-scale velocity field. Note that for multi-phase flow, the transmissibilities and the fine-scale basis functions must be recomputed in regions of significant mobility change.

6. Numerical studies

In order to demonstrate the performance of the MSFV method, we present numerical studies with a broad range of permeability fields. The first test case deals with a homogeneous permeability distribution; the permeability field for the second one is random. Geostatistically generated permeability fields are employed in the remaining examples. Fields with high variability as well as isotropic and anisotropic correlation structures are examined.

6.1. Test case

For all the following studies we consider the same configuration with different permeability fields. The physical domain is $[0,1] \times [0,1]$, an injector is located at $(1/12, 1/12)$ and a producer at $(11/12, 11/12)$. The injection and production rates are -1 and 1, respectively. Fig. 4 shows the 30×30 fine grid (thin lines) which carries the permeability field. The bold lines represent the coarse 5×5 grid which is used for the coarse-scale computation. For the results presented in this section we used the fine-scale basis functions Φ to reconstruct the fine-scale pressure and velocity fields from the coarse solution. Henceforth, when we refer to a multi-scale (MS) solution we mean the fine-scale solution reconstructed from the coarse solution.

We use particle tracking to evaluate the accuracy of the reconstructed velocity fields. Although not an efficient way to solve transport problems, particle tracking is very sensitive and is well suited to study the quality of the velocity field. Fig. 5 shows the initial uniform distribution within the computational domain. To minimize errors due to the well location, we exclude the coarse volume containing the injector. We

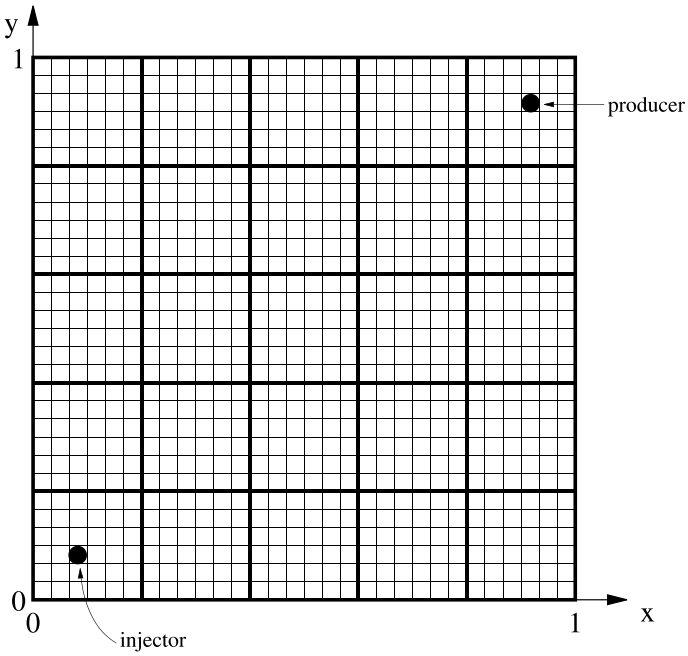

Fig. 4. 30×30 fine grid (thin lines) with 5×5 coarse grid (bold lines).

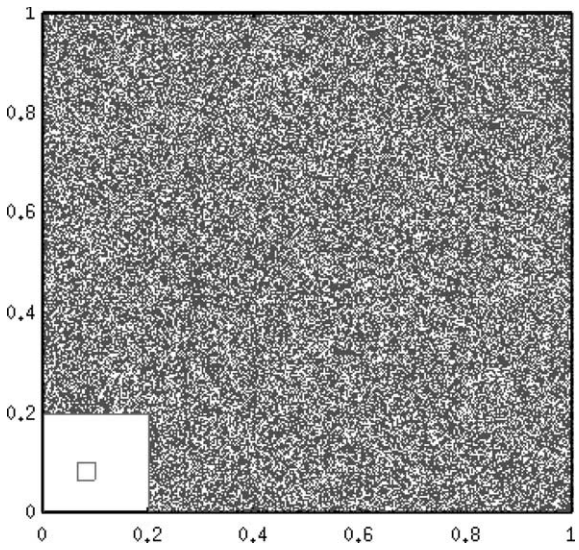

Fig. 5. Tracer particles at initial time.

found that except close to the wells, the pressure field is not very sensitive to the location of the well within a coarse volume. In all the following scatter plots the wells are shown by dark squares which have the size of a volume. We note that resolution of the fine-scale behavior near the well requires special handling and will be addressed in later papers.

6.2. Homogeneous permeability field

Fig. 6 shows the fine and MS pressure solutions (thin and bold isolines, respectively) for a homogeneous permeability field with $K \equiv 1$. This simple case proves that the MSFV method also has potential as a highly accurate numerical method even in the absence of a complex permeability structure.

6.3. Random permeability field

The permeability distribution for this test case is given by $K = 0.1 + 50(1 + \sin(10(x + y)))\xi$ (as shown in Fig. 7(a)), where ξ is a random variable equally distributed between 0 and 1. Fig. 7(b) shows the pressure isolines of the fine and MS solutions (thin and bold lines, respectively). It can be seen that the two solutions are very close, and that the pressure levels are accurately predicted by the MS solution. Figs. 8(a) and (b) show tracer particles after 0.5 pvi for the fine and MS velocity fields, respectively. The ability of the MS solution to reproduce the small structures of the tracer front is remarkable.

We now demonstrate the importance of a divergence free fine-scale velocity field. Fig. 9 shows the tracer particles after 0.5 pvi as before, but the fine-scale velocity field was constructed using the dual basis functions $\tilde{\Phi}$, instead of the fine-scale basis Φ. Since this velocity field is not continuous, the particles bunch up and most of the information about the front is lost. This may not be as important, if a hyperbolic continuum equation is solved instead. It is evident, however, that mass balance errors occur at the fine scale, unless we ensure that the fine-scale velocity is conservative.

6.4. Permeability field with isotropic correlation structure

The permeability field for this test case was generated geostatistically. The mean and variance of $\log(K)$ are 0 and 3, respectively. The correlation structure is isotropic with $l_x = l_y = 0.3$, where l is the correlation length. Fig. 10 shows the permeability field. The scatter plots in Fig. 11 show the tracer particles after 0.2 pvi (the fine solution in the left and the MS solution in the right plot). As in the previous examples, it can be observed that the velocity field of the MS solution compares very well with the fine solution.

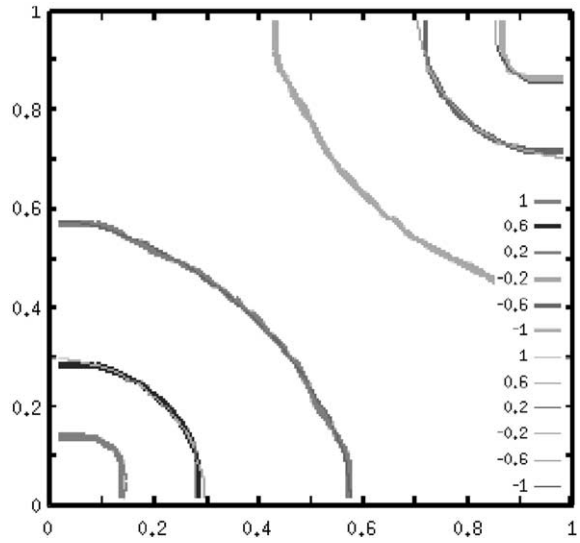

Fig. 6. Pressure isolines from the example in Section 6.2: bold lines from the MS solution, thin lines from the fine solution.

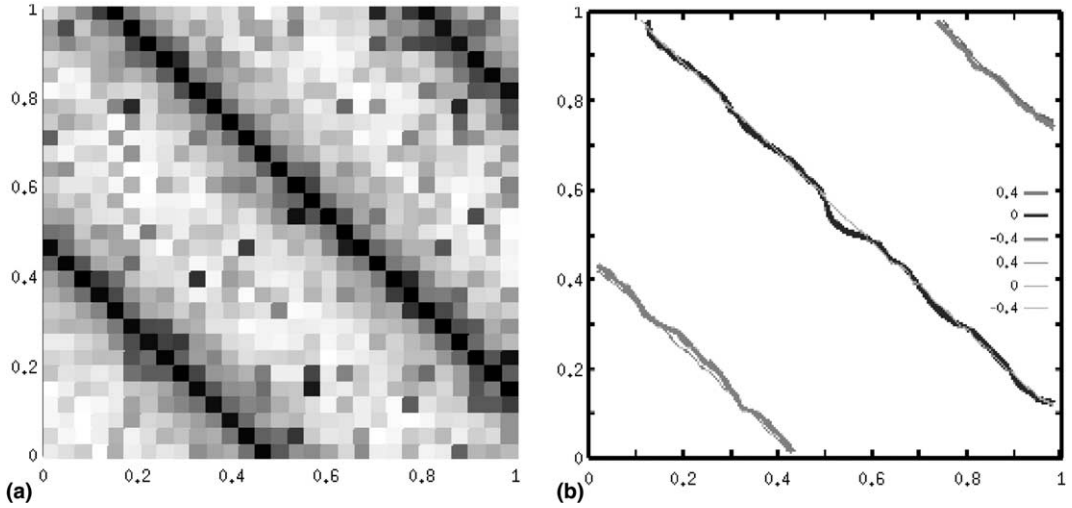

Fig. 7. From the example in Section 6.3: (a) permeability field, (b) pressure isolines; bold lines from the MS solution, thin lines from the fine solution.

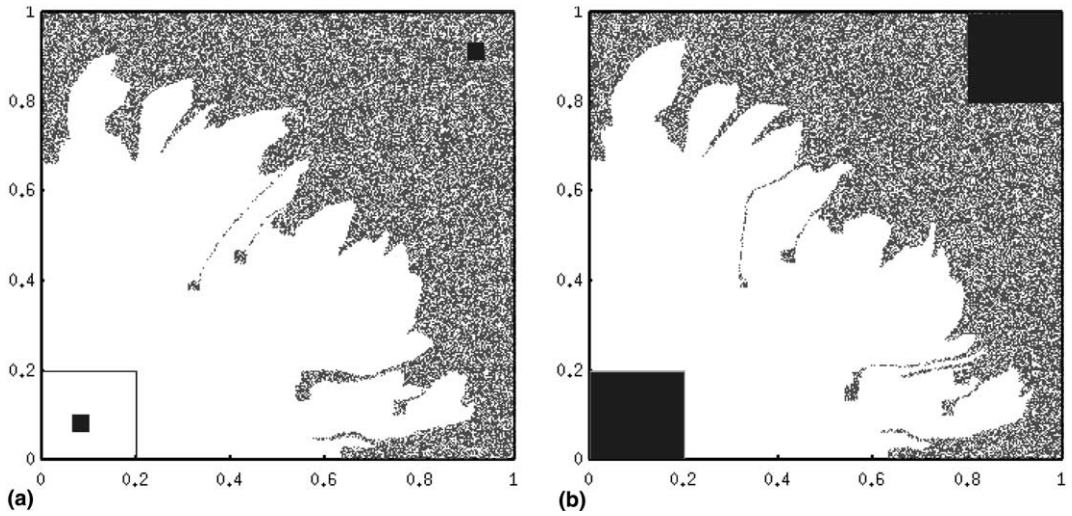

Fig. 8. Tracer particles after 0.5 pvi from the example in Section 6.3: (a) fine solution on a 30×30 grid, (b) MS solution with a 5×5 coarse grid; the dark squares mark the wells.

6.5. Permeability field with anisotropic correlation structure

In this example, we consider a geostatistically generated permeability field with $l_x = 0.3$, $l_y = 0.03$ and for which the mean and variance of $\log(K)$ are 0 and 9, respectively. The field is shown in Fig. 12. Scatter plots after 0.2 and 0.4 pvi are presented in Figs. 13 and 14, respectively. In both figures, the fine solution is in the left plot and the MS solution is in the right plot. Again, the agreement is excellent. It can be seen that in some volumes the particles hardly evolved which is due to the high variance of the permeability field.

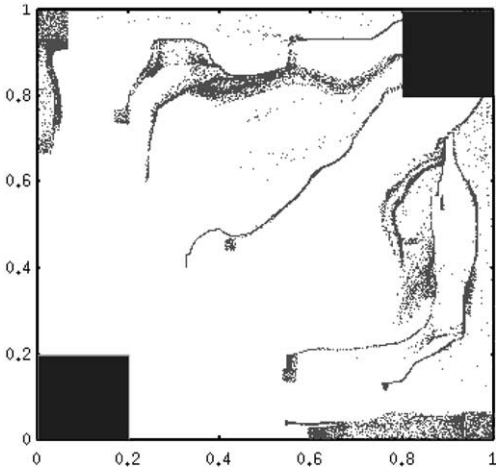

Fig. 9. Tracer particles after 0.5 pvi from the example in Section 6.3: MS solution on a 5×5 coarse grid, here the reconstructed fine-scale velocity field is not divergence free.

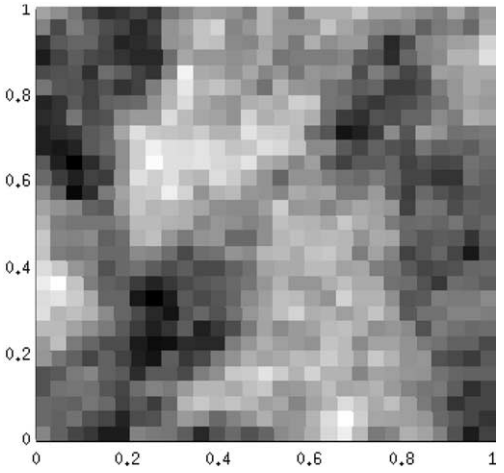

Fig. 10. Permeability field from the example in Section 6.4.

Upscaling of such low permeability regions opens the possibility of actually upscaling small geometrical features of a reservoir.

In the next example the permeability field has a longer correlation structure with $l_x = 0.03$ and $l_y = 0.6$. The mean and variance of $\log(K)$ are 0 and 3, respectively. Fig. 15 shows the permeability field. Some discrepancy between the fine and MS solution can be observed in Fig. 16 which shows the scatter plots after 0.2 pvi. In the MS solution (right plot) it can be seen that the thin finger in the center of the domain is slightly longer than in the fine solution (left plot). Later, at breakthrough, the agreement is much better, as shown in Fig. 17.

The test cases presented in this section confirm the excellent agreement of the MS solution with the fine solution for a broad range of permeability fields. Our numerical studies demonstrate that the MSFV

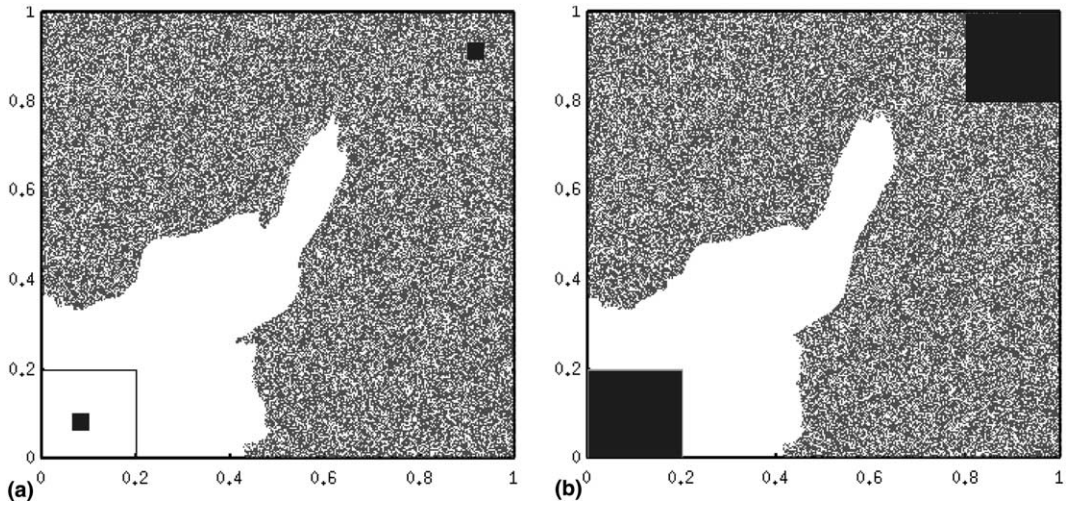

Fig. 11. Tracer particles after 0.2 pvi from the example in Section 6.4: (a) fine solution on a 30×30 grid, (b) MS solution with a 5×5 coarse grid; the dark squares mark the wells.

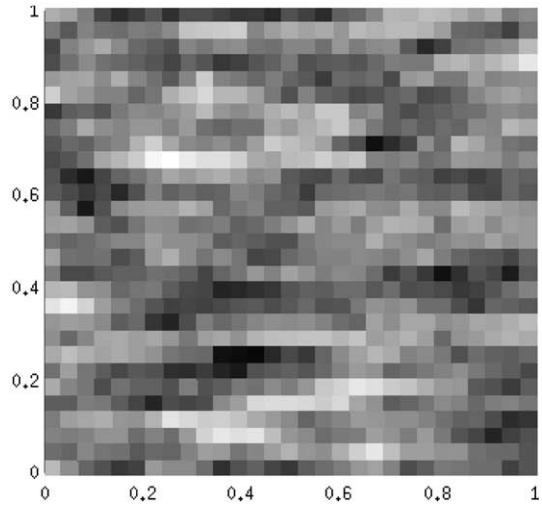

Fig. 12. Permeability field from the first example in Section 6.5.

method not only yields accurate coarse fluxes, but it also allows for reconstructing a fine-scale velocity field with proper divergence behavior. Particle tracking studies as well as pressure contour maps demonstrate the excellent agreement between the MS and fine solutions for a broad range of test cases.

7. Discussion

We have demonstrated that the MSFV method is very powerful for problems of single-phase flow on structured grids. Next, convergence studies show that the MSFV method is consistent with the fine

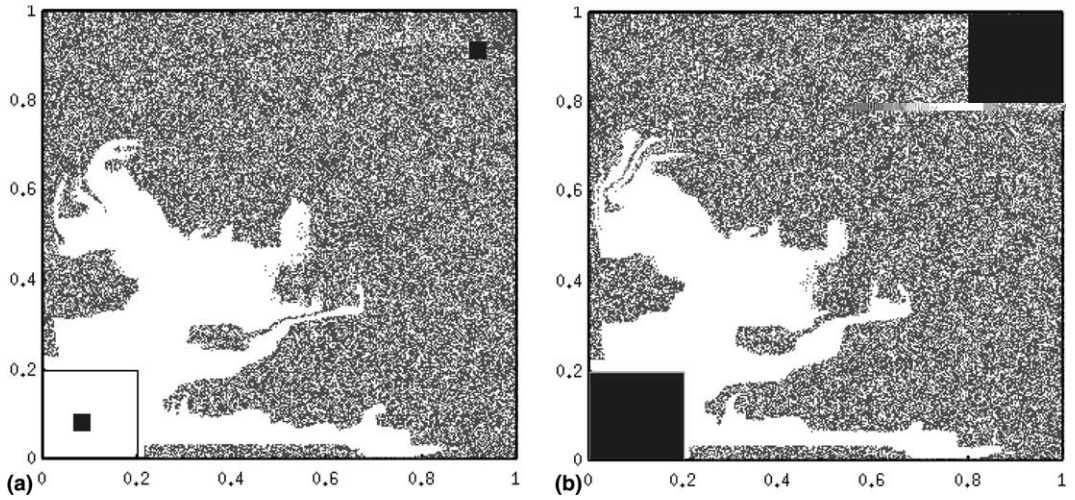

Fig. 13. Tracer particles after 0.2 pvi from the first example in Section 6.5: (a) fine solution on a 30×30 grid, (b) MS solution with a 5×5 coarse grid; the dark squares mark the wells.

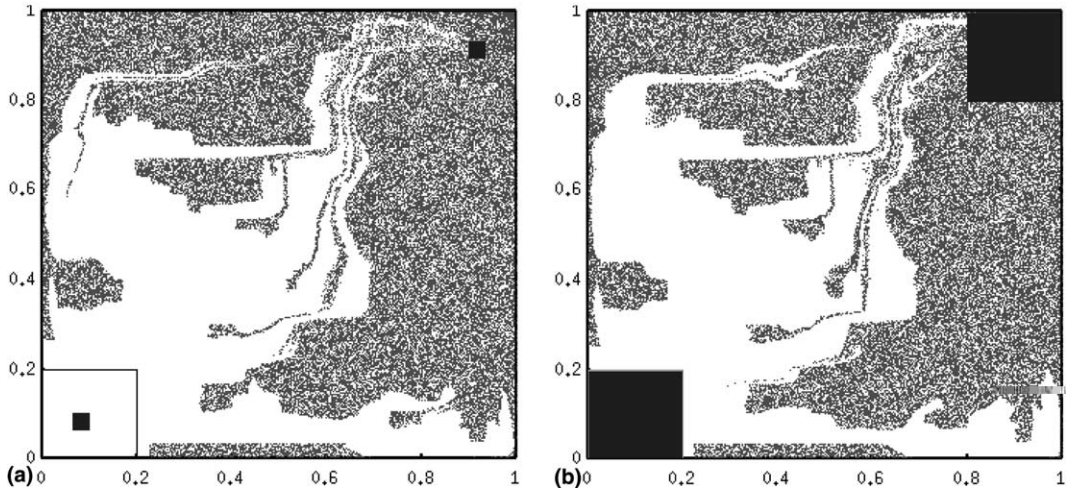

Fig. 14. Tracer particles after 0.4 pvi from the first example in Section 6.5: (a) fine solution on a 30×30 grid, (b) MS solution with a 5×5 coarse grid; the dark squares mark the wells.

solution. Furthermore, we explain how the MSFV method can be extended for unstructured grids and multi-phase flow problems.

7.1. Convergence

The convergence as the small scale approaches zero is an important property in homogenization-related studies. In our problems, however, the limit is the discrete fine-scale problem which is captured exactly when the coarse grid employed by the MSFV method coincides with the given fine grid. We studied the

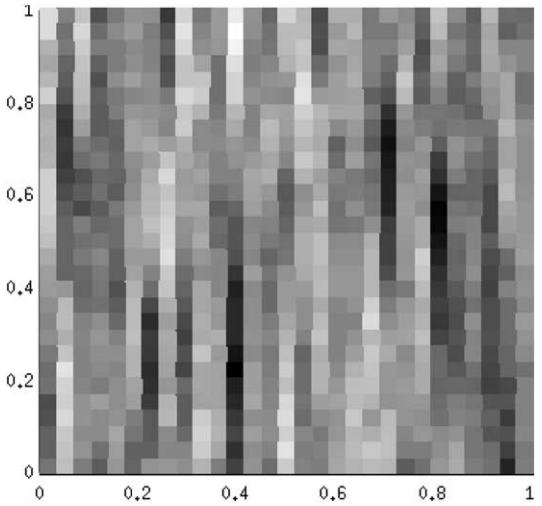

Fig. 15. Permeability field from the second example in Section 6.5.

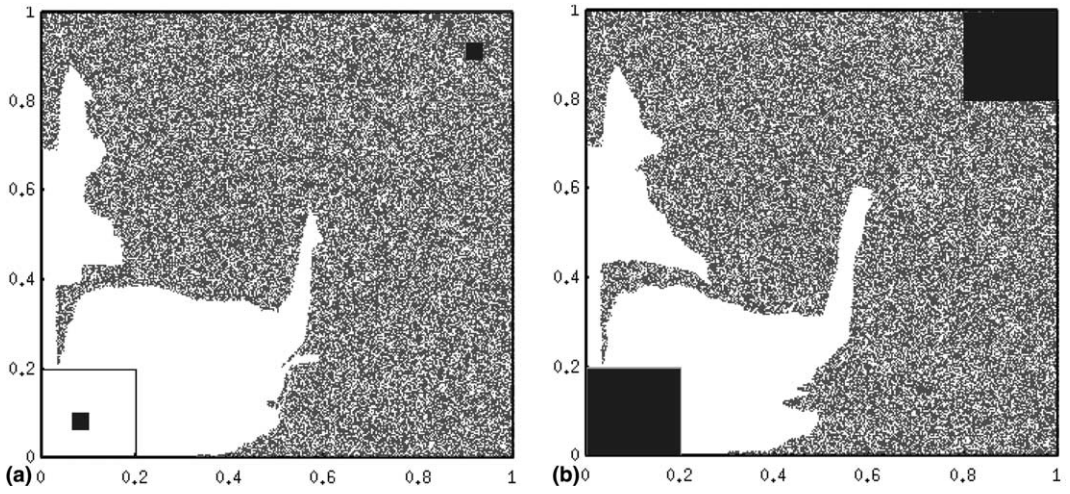

Fig. 16. Tracer particles after 0.2 pvi from the second example in Section 6.5: (a) fine solution on a 30×30 grid, (b) MS solution with a 5×5 coarse grid; the dark squares mark the wells.

convergence behavior of the MSFV method as a function of coarse-grid resolution. We present the results for a test case similar to the one explained in Section 6.1 (Fig. 4). The permeability field has a correlation structure with $l_x = 0.03$ and $l_y = 0.6$ and the mean and variance of $\log(K)$ are 0 and 3, respectively (Fig. 18 shows the permeability field). We used a fine grid with a resolution of 100×100. The error of a MS solution is defined as the infinity norm of the difference between the fine and the MS pressure solution, normalized by the pressure range in the fine solution. Fig. 19 shows the error for coarse grids with 50×50, 25×25, 10×10 and 5×5 volumes. It can be observed that the multi-scale solution converges, as the coarse grid is refined. Fig. 19 also indicates that the error remains very small up to a coarsening factor of approximately 10, but then increases substantially. Certainly, the appropriate level of coarsening is problem-dependent.

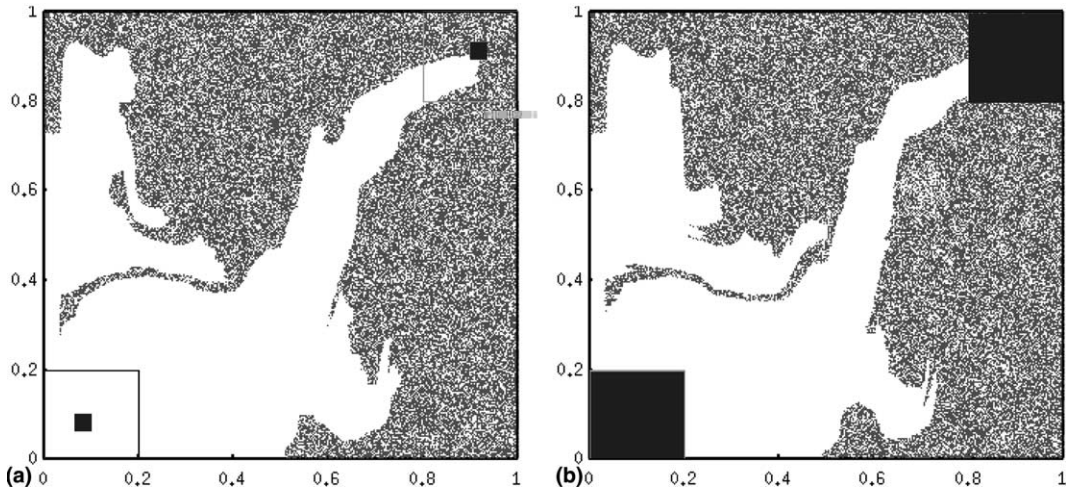

Fig. 17. Tracer particles after 0.4 pvi from the second example in Section 6.5: (a) fine solution on a 30×30 grid, (b) MS solution with a 5×5 coarse grid; the dark squares mark the wells.

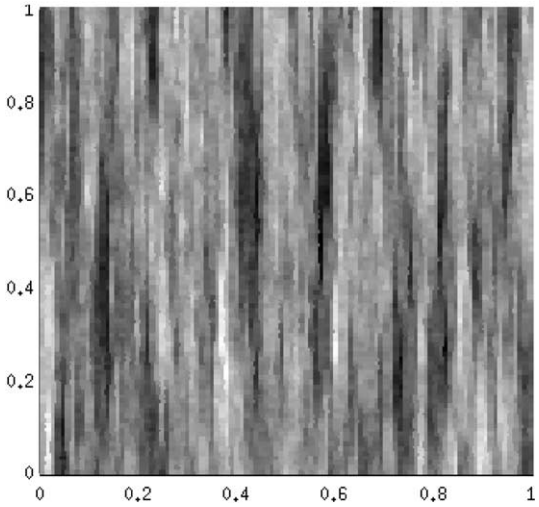

Fig. 18. Permeability field.

7.2. Unstructured grids

Although the MSFV method is explained for structured grids, the extension for unstructured grids is straightforward. Again, for simplicity we explain everything in 2D, but the ideas are the same for 3D. First we discuss how to map a permeability field from a fine grid onto any coarse grid which is a necessary step to deal with unstructured grids.

In many cases the permeability field is represented on a fine grid which is not aligned with the computational grid and has to be mapped. Here, we describe an oversampling technique proposed by Hou and Wu [8]. Although designed to overcome grid resonance effects, this technique allows mapping a perme-

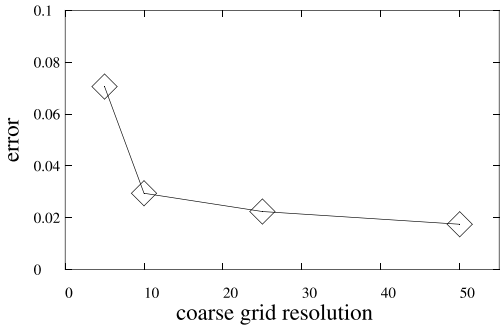

Fig. 19. Infinity norm of the pressure error for coarse grids with 5×5, 10×10, 25×25 and 50×50 volumes.

ability field from one grid onto another. This is illustrated in Fig. 20, which shows a fine permeability grid (thin lines) that is misaligned with a coarse computational grid (bold lines). Also shown is the dual grid (dashed bold lines) and one of the dual control volumes (light dark color). In order to get the dual basis functions associated with volumes 1–4, we first solve for the four intermediate basis functions $\tilde{\Psi}^{a,b,c,d}$ in the dark region. The dual basis functions $\tilde{\Phi}^i$ $(i = 1, 4)$ are then obtained from the linear combination

$$\Phi^i = \sum_{j \in \{a,b,c,d\}} c_{ij} \Psi^j \quad \text{for } 1 \leqslant j \leqslant 4, \tag{18}$$

where c_{ij} are the constants determined by the condition $\Phi^i(\mathbf{x}^j) = \delta_{ij}$. Note that the dual basis functions constructed with the oversampling method may be discontinuous at the element boundaries. In general,

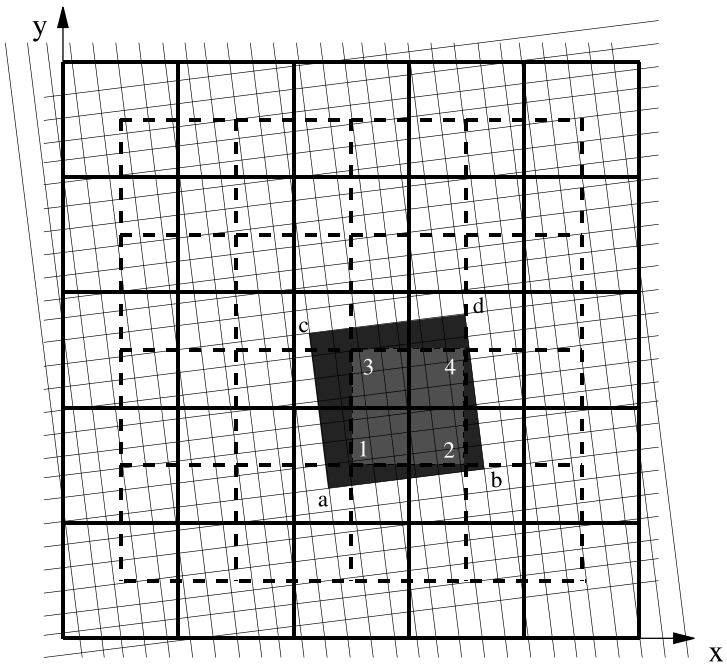

Fig. 20. Oversampling to map the permeability field from a fine grid (thin lines) onto a coarse computational grid (bold lines); the dashed bold lines show the dual grid; also shown is one of the dual control volumes (light dark color) and a corresponding oversampling region.

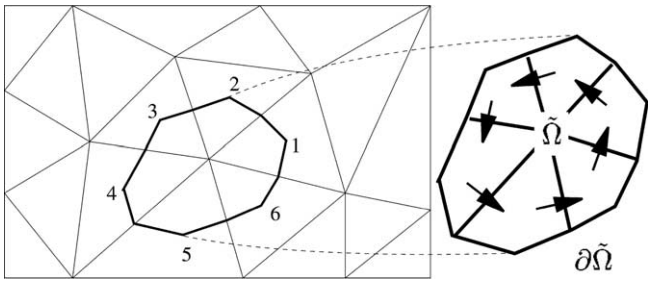

Fig. 21. Coarse unstructured 2D grid with dual volume $\tilde{\Omega}$.

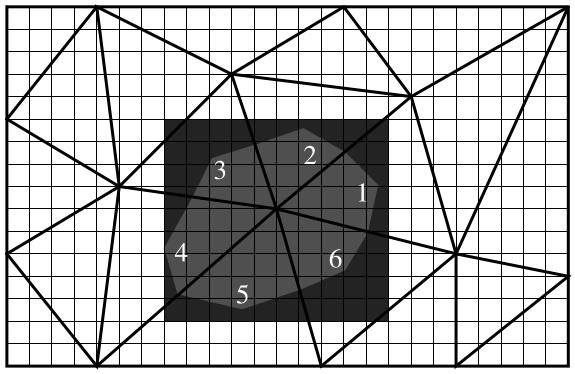

Fig. 22. Unstructured grid (bold lines) with a dual control volume (light gray region); shown is also the corresponding oversampling domain (dark region) on which the elliptic problems are solved (one for each of the six cells).

however, oversampling reduces the effects of the imposed boundary conditions on the computed dual basis functions.

Fig. 21 shows an unstructured grid (thin lines) with a dual control volume $\tilde{\Omega}$ (bold lines). To compute the transmissibilities one can apply the same procedure as for structured grids combined with the oversampling technique, but now six volumes (volumes 1–6) are involved for the dual control volume. Fig. 22 shows the dual control volume (light dark region) and the underlying fine grid. The dark region is the corresponding oversampling domain on which the elliptic problems are solved (one for each of the six cells).

7.3. Multi-phase flow

We briefly want to discuss what has to be considered for the elliptic problem, if multi-phase flow is involved. Here we do not address the multi-scale transport problem. For generality we make the assumption that the saturation field is updated on a fine-scale grid.

With more than one phase, the tensor λ in Eq. (1) becomes a function of the saturation. Therefore, the local elliptic problems, which determine the dual basis functions, change with time. Nevertheless, the transmissibilities and the fine-scale basis functions have to be recomputed only for those volumes where the saturation gradients change. This is illustrated in Fig. 23 which shows a saturation front propagating through a domain discretized by a 15×15 coarse grid. The refined grid near the front indicates that for the corresponding control volumes, the dual basis functions have to be recomputed in order to account for changes of the mobility field. Since in general only a small fraction of a reservoir is affected by large changes

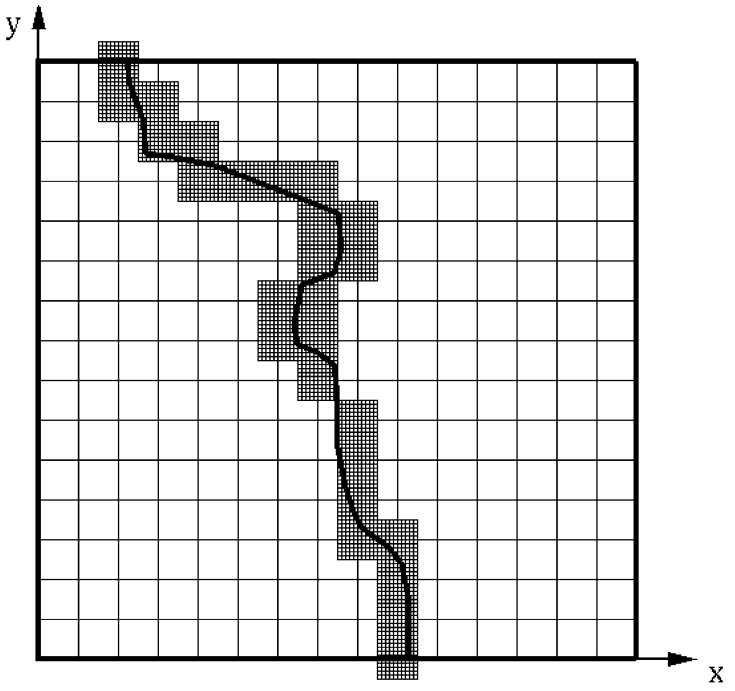

Fig. 23. Adaptation by recomputing the transmissibilities and the fine-scale basis functions near the saturation front.

in the saturation field, computation of the transmissibilities and reconstruction of the fine-scale basis functions is expected to be small in terms of computational effort.

8. Conclusions

A new multi-scale finite-volume method for elliptic problems describing flow in porous media has been developed, tested and analyzed. The method, which is based on a flux-continuous finite-difference approach, is conservative and treats full tensor permeabilities and nonorthogonal grids correctly. The calculated transmissibilities account for the fine-scale effects. Once they are computed, these transmissibilities can be used by any finite-volume code that can handle multi-point flux discretizations. Specifically constructed fine-scale basis functions allow for reconstructing a fine-scale velocity field that is conservative. The construction of the transmissibilities and of the fine-scale basis functions can be done in parallel and has to be done once only. We outlined how the ideas can be extended to unstructured grids and multi-phase flow. Finally, various numerical examples demonstrate the accuracy of the method and tracer particle studies show that the fine-scale velocity field can be reconstructed accurately from the coarse solution. The extra computational effort compared with coarse-scale simulations is mainly due to a preprocessing step and becomes insignificant after a large number of time steps.

Acknowledgements

This work has been supported by ChevronTexaco Exploration and Production Technology Company and ChevronTexaco/Schlumberger Intersect Alliance Technology.

References

[1] T. Arbogast, Numerical subgrid upscaling of two phase flow in porous media, Technical Report, Texas Institute for Computational and Applied Mathematics, The University of Texas at Austin, 1999.
[2] T. Arbogast, S.L. Bryant, Numerical subgrid upscaling for waterflood simulations, SPE 66375, presented at the SPE Symp. on Reservoir Simulation, Houston, 2001.
[3] R. Beckie, A.A. Aldama, E.F. Wood, Modeling the large-scale dynamics of saturated groundwater flow using spatial filtering, Water Resour. Res. 32 (1996) 1269–1280.
[4] Z. Chen, T.Y. Hou, A mixed finite element method for elliptic problems with rapidly oscillating coefficients, Math. Comput. 72 (2003) 541–576.
[5] L.J. Durlofsky, Numerical calculation of equivalent grid block permeability tensors for heterogeneous porous media, Water Resour. Res. 27 (1991) 699–708.
[6] Y. Efendiev, T. Hou, X. Wu, Convergence of a nonconformal multiscale finite element method, SIAM J. Numer. Anal. 37 (2000) 888–910.
[7] Y. Efendiev, X. Wu, Multiscale finite element for problems with highly oscillatory coefficients, Numer. Math. 90 (2002) 459–486.
[8] T. Hou, X.H. Wu, A multiscale finite element method for elliptic problems in composite materials and porous media, J. Comp. Phys. 134 (1997) 169–189.
[9] P. Jenny, C. Wolfsteiner, S.H. Lee, L.J. Durlofsky, Modeling flow in geometrically complex reservoirs using hexahedral multi-block grids, SPE J. (2002) 149–157.
[10] S.H. Lee, L.J. Durlofsky, M.F. Lough, W.H. Chen, Finite difference simulation of geologically complex reservoirs with tensor permeabilities, SPERE&E (1998) 567–574.
[11] S.H. Lee, H. Tchelepi, P. Jenny, L. Dechant, Implementation of a flux continuous finite-difference method for stratigraphic, hexahedron grids, SPE J. (2002) 269–277.
[12] T.C. Wallstrom, T.Y. Hou, M.A. Christie, L.J. Durlofsky, D.H. Sharp, in: Application of a New-phase Upscaling Technique to Realistic Reservoir Crosssections, SPE51939, Presented at the SPE Symp. on Reservoir Simulation, Houston, 1999.